

Long range avalanche-like electron heat transport events in the low confinement mode tokamak plasma experiment

M. J. Choi,^{1, a)} M. H. Woo,¹ J.-M. Kwon,¹ S. H. Ko,¹ H. Jhang,¹ H. K. Park,² T. S. Hahm,³ H. S. Kim,¹ J. Lee,¹ M. Kim,² G. S. Yun,⁴ and the KSTAR team

¹⁾*National Fusion Research Institute, Daejeon 34133, Korea*

²⁾*Ulsan National Institute of Science and Technology, Ulsan 689-798, Korea*

³⁾*Seoul National University, Seoul, Korea*

⁴⁾*Pohang University of Science and Technology, Pohang, Gyungbuk 790-784, Korea*

(Dated: 14 December 2024)

Long range avalanche-like electron heat transport events are observed in the L-mode tokamak plasma experiment. Detail avalanche dynamics and characteristics of the electron temperature (T_e) fluctuations have been revealed by virtue of the advanced T_e imaging diagnostics in the KSTAR tokamak. Initially, the jet-like T_e corrugations appear in the wake of the preceding avalanche-like event. The long range avalanche-like electron heat transport event occurs when the T_e corrugations disappear with the $m = 1$ mode and the T_e fluctuation power increases. The avalanche dynamics is slightly different depending on characteristics of the associated T_e fluctuation, but the common T_e gradient-correlated-fluctuation with the power law spectrum $S(f) \propto f^{-0.7}$ and the Hurst exponent $H \sim 0.8$ is observed. This implies that the nondiffusive avalanche-like transport events are a dominant electron heat transport process in the L-mode plasma when the significant MHD instabilities are absent.

^{a)}mjchoi@nfri.re.kr

Tokamaks are a device to confine a hot and dense plasma with a strong magnetic field of the nested structure for fusion. Understanding characteristics of the cross-field transport is one of the most fundamental problems in tokamak plasmas. Among various transport processes the turbulence transport has been an important issue for many years, but characteristics of the turbulence transport is not fully understood yet and controversial, i.e. whether it is local/nonlocal or diffusive/nondiffusive.

As one of the nondiffusive heat transport process, long range avalanches are suggested^{1,2} and studied via gyrokinetic simulations³⁻⁷. Gyrokinetic simulations have improved understanding of avalanche dynamics such that long range avalanches can occur only when the self-organizing $E \times B$ shear flow layers are destroyed, which could explain a beneficial confinement scaling with a machine size⁶. This avalanche dynamics is found to be working in the electron heat channel as well as the ion heat channel, though the formation mechanism of $E \times B$ shear flow layers can be different⁸. Unfortunately, experimental observation of long range avalanches is rare^{9,10} and detail avalanche dynamics has been missing. This is mainly due to lack of a diagnostics which can measure temperature variations with a sufficient spatio-temporal resolution.

In this paper, we provide the first experimental observation of detail avalanche dynamics by virtue of the advanced electron temperature (T_e) imaging diagnostics in the KSTAR tokamak. Initially, the jet-like mesoscale T_e corrugations appear. Note that the jet-like T_e corrugations can be indicators of the $E \times B$ shear flow layers if the T_e gradient-associated-turbulence is prevailing and regulated by the $E \times B$ shear flow layers. Indeed, it is found that the T_e gradient-correlated-fluctuation with the power law spectrum $S(f) \propto f^{-0.7}$ is prevailing during the avalanching periods in this plasma. More importantly, long range avalanche-like electron heat transport event occurs after the jet-like T_e corrugations are destroyed and the associated T_e fluctuation power increases. The quiescent magnetic fluctuation during the avalanching periods suggests that this event is distinguished from the MHD instabilities. The avalanche dynamics changes slightly depending on characteristics of the associated T_e fluctuation.

The KSTAR discharge #13728 is a limiter low confinement mode (L-mode) plasma with the major radius $R_0 = 1.8$ m, the minor radius $a \sim 0.4$ m, the elongation $\kappa \sim 1.4$, the triangularity $\delta \sim 0.3$, and the monotonic safety factor q profile ($q_{95} \sim 7$ at the 95% normalized poloidal flux). Total 4 MW neutral beam injections (NBI) are applied to heat the plasma.

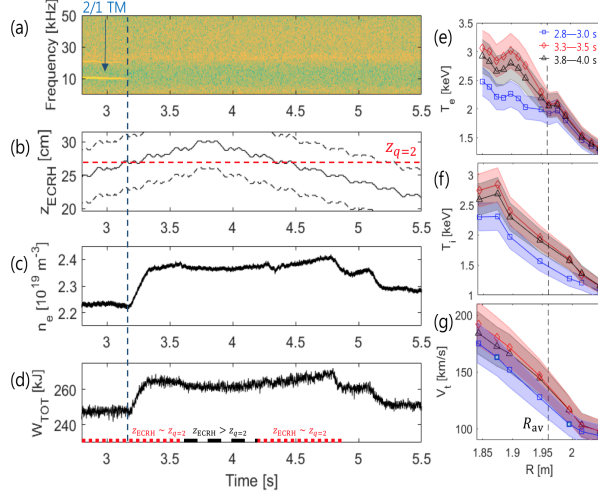


FIG. 1. (Color online) (a) Power spectrum of magnetic fluctuations. (b) The vertical target position of the ECRH z_{ECRH} (bold line) and effective deposition widths (black dashed lines). Red dashed line indicates the expected $q = 2$ surface location $z_{q=2}$. (c) Line averaged electron density (n_e). (d) Total stored energy (W_{TOT}). Red dotted lines indicate the $z_{\text{ECRH}} \sim z_{q=2}$ period, and black dashed line indicates the $z_{\text{ECRH}} > z_{q=2}$ period. (e)–(g) The average electron temperature (T_e), ion temperature (T_i), and toroidal velocity (V_t) profiles in different periods, respectively.

An $m/n = 2/1$ tearing mode (TM) was destabilized in the plasma current ramp-up phase. Power spectrum of magnetic fluctuations measured by a Mirnov coil¹¹ is shown in figure 1(a). An ~ 10 kHz signal and its second Fourier harmonics are originated from the TM. 1 MW electron cyclotron resonance heating (ECRH) was launched to stabilize the TM. As shown in figure 1(b), the approximated ECRH vertical target position z_{ECRH} at the resonant major radius $R_{\text{ECRH}} \sim 1.8$ m has been swept. The TM signal disappears near $t = 3.17$ s when the z_{ECRH} is expected to be close to the z position of the $q = 2$ flux surface at $R = R_{\text{ECRH}}$.

After the $2/1$ TM is suppressed or reduced undetectably small, the plasma stored energy is significantly improved. The plasma has the larger stored energy and the profiles are also steeper when the z_{ECRH} is closer to the $q = 2$ flux surface as shown in figure 1(d)–(g). Note that T_e profiles are measured by the 1D absolutely calibrated electron cyclotron emission (ECE) diagnostics¹², and the T_i and V_t profiles were estimated from the charge exchange spectroscopy (CES) diagnostics using carbon impurity¹³.

Long range avalanche-like electron heat transport events occur without any external perturbations when the significant MHD instabilities are absent in this plasma. The 1D ECE

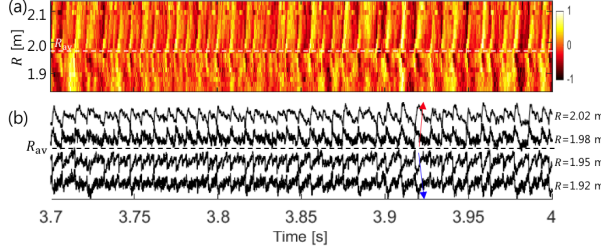


FIG. 2. (Color online) (a) The spatio-temporal pattern of the rescaled normalized T_e fluctuation in the $z_{\text{ECRH}} > z_{q=2}$ period. (b) The rescaled normalized T_e fluctuations measured at four different R s. Bumps ($\delta T_e > 0$) propagate outwards in $R > R_{\text{av}}$ (downhill) and voids ($\delta T_e < 0$) propagate inwards in $R < R_{\text{av}}$ (uphill).

diagnostics and two independent 2D electron cyclotron emission imaging (ECEI) diagnostics¹⁴ installed at different toroidal angles separated by 22.5 degrees are used to measure T_e evolution during the events. A spatial resolution of the ECEI diagnostics is about 2 cm in radial and 3 cm in vertical direction and a temporal resolution is 2 μs . The illustration of the diagnostics view is shown in figure 3(a).

Detail avalanche dynamics is slightly different between the $z_{\text{ECRH}} \sim z_{q=2}$ period and the $z_{\text{ECRH}} > z_{q=2}$ period. First, figure 2 shows the relatively simpler events observed in the $z_{\text{ECRH}} > z_{q=2}$ period. Figure 2(a) is the spatio-temporal pattern of the normalized T_e fluctuation ($\tilde{T}_e \equiv (T_e - \langle T_e \rangle) / \langle T_e \rangle$ where $\langle \rangle$ means the time average) measured by ECE channels at different R s. \tilde{T}_e from four ECE channels are plotted in figure 2(b). Voids ($\delta T_e = T_e - \langle T_e \rangle < 0$) and bumps ($\delta T_e > 0$), propagating inwards and outwards from $R_{\text{av}} \sim 1.96$ m, are observed over the broad radial region. Rough estimation of the propagation speed is about 30–100 m/s, which is much faster than a general diffusive process. Note that each \tilde{T}_e is rescaled to be in the -1 to 1 range in figure 2.

The two-dimensional (2D) T_e dynamics is more instructive as shown in the $\delta T_e = T_e - \langle T_e \rangle$ images in figure 3(c) for one event near $t = 3.92$ s. Vertical cuts along the plasma center are shown in figure 3(d) to help to understand the images. After the preceding event finished, the poloidally symmetric jet-like patterns appear as in the frame #1 in figure 3(c) and (d). The jet-like patterns in δT_e represent that the T_e profile (and the T_e gradient) is radially corrugated. Spacing between the local maximums of the T_e gradient is roughly 10 cm ($\sim 40\rho_i$ where $\rho_i \sim 0.24$ cm). Note that the most probable spacing observed in the recent gyrokinetic

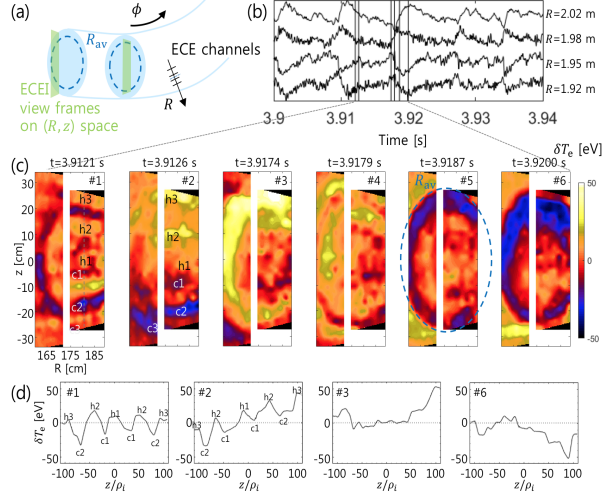


FIG. 3. (Color online) (a) The illustration of the diagnostics view. (b) The rescaled normalized T_e fluctuations. (c) δT_e images obtained by the ECEI diagnostics during a single avalanche-like event. (d) Vertical cut of δT_e images along the plasma center at the corresponding frame in (c). h1–h3 and c1–c3 indicate positive and negative δT_e jets, respectively.

simulations¹⁵ is $\sim 40\rho_s = 40\sqrt{T_e/T_i}\rho_i$. Next, these symmetric δT_e jets are perturbed by a larger scale $m = 1$ δT_e mode as shown in the frame #2. The large $m = 1$ mode has the peak at the top and the valley at the bottom (the $\sin\theta$ behaviour). The δT_e jets become tilted in the vertical cut, and they move downwards about $\sim 10\rho_i$ within $500\ \mu\text{s}$. As a side note, the δT_e polarities of the jets in the frame #1 and the $m = 1$ mode in the frame #2 are correlated and the opposite patterns with the $-\sin\theta$ mode are also observed. The $m = 1$ mode becomes clear, as the δT_e jets become blurred within a millisecond. In next a few milliseconds the $m = 1$ mode is dominant (between the frame #2 and #3). The local T_e near R_{av} increases significantly in a few milliseconds before the avalanche-like event as in the frame #3. An δT_e void in the $R < R_{av}$ region and a bump in the $R > R_{av}$ region are created and propagate inwards and outwards, respectively, from the frame #4 to #6.

The long range avalanche-like event occurs when the T_e profile corrugations, which can be indicators of $E \times B$ shear flow layers, are destroyed. The measured spacing of the T_e profile corrugations ($\sim 40\rho_i$) agrees quantitatively with the recent gyrokinetic simulation result¹⁵. The T_e profile corrugation can result from ∇T_e -associated-turbulence regulation by $E \times B$ shear flow layers. Although measurements of $E \times B$ shear flow layers were not available due to its short life time, we found that ∇T_e -correlated-fluctuation prevails in the avalanching

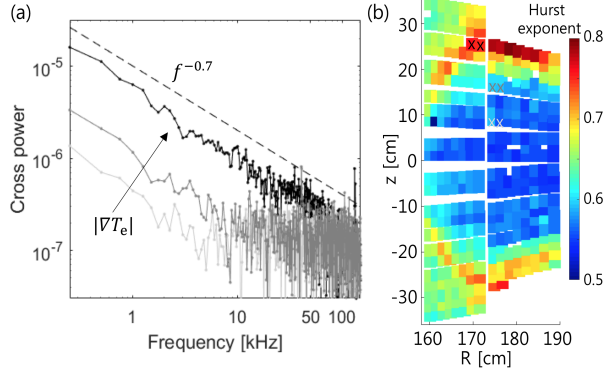


FIG. 4. (Color online) (a) The cross power spectrum measured by two adjacent ECEI channels in the $z_{\text{ECRH}} > z_{q=2}$ period. Black, grey, and light grey spectra are obtained by the channels marked by X with the corresponding colors in (b), respectively. (b) The 2D Hurst exponent measurements from \tilde{T}_e .

periods.

Figure 4(a) shows the cross power spectrum measured by pairs of two adjacent ECEI channels for the $z_{\text{ECRH}} > z_{q=2}$ period ($t = 3.7\text{--}4.0$ s). The cross power spectrum near R_{av} where the avalanche initiates and the T_e gradient is largest shows a significant fluctuation power up to 75 kHz (black). As going far from R_{av} , the T_e gradient is reduced and the weaker fluctuation is observed (grey and light grey). More clear evidence for correlation between the fluctuation power and the T_e gradient is shown in figure 7(b). The channels near R_{av} are used to measure slow temporal evolution of the 1–75 kHz fluctuation amplitude (black dot) as the $|\nabla T_e|$ (black dashed line) changes slightly in time. The 1–75 kHz fluctuation amplitude is well correlated with the local $|\nabla T_e|$ just inside R_{av} . Note that the 0–1 kHz range is excluded in the fluctuation amplitude measurement to safely avoid possible effects from secular movements of the plasma (10–100 ms time scale).

In addition, investigation of fast temporal evolution of the ∇T_e -correlated-fluctuation power found that its evolution is related to the avalanche dynamics. In order to estimate the fast temporal evolution accurately, two ECEI channels close to R_{av} (indicated as black X marks in figure 4(b)) are used. The \tilde{T}_e signals of 1 ms length from the two channels are filtered by the 1–75 kHz bandpass filter, and the RMS of their cross correlation, i.e. the cross power (C_{T_e}), is calculated. Figure 5(b) shows the result: it increases a few milliseconds before the events and decreases after the events when the $E \times B$ shear flow layers are thought

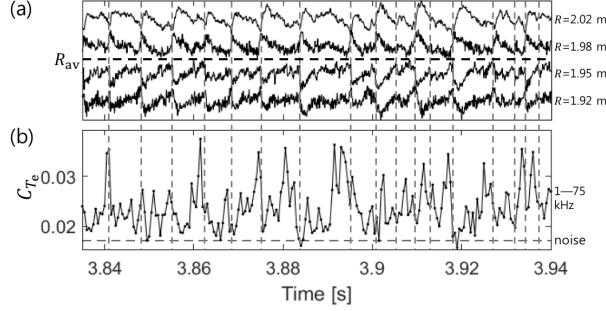


FIG. 5. (a) The rescaled normalized T_e fluctuations in the $z_{\text{ECRH}} > z_{q=2}$ period. (b) Fast temporal evolution of the correlated T_e fluctuation power in the 1–75 kHz frequency band.

to appear. This implies that the ∇T_e -correlated-fluctuation itself can play a role in triggering the avalanche-like event as well as that the fluctuation might be regulated by the $E \times B$ shear flow layers.

Another important thing to note is that the cross power spectrum in figure 4(a) follows $f^{-0.7}$, i.e. the power law. The power law spectrum $S(f) \propto f^{-(2-\alpha)} = f^{-0.7}$ with $0 < \alpha = 1.3 < 2$ implies that the nondiffusive avalanche-like events are a dominant electron heat transport process in this plasma. Based on observations of the long range avalanche-like events and the power law spectrum, one may ask whether the plasma is in the self-organized criticality (SOC) state¹⁶. Detail investigation of the SOC behaviours in the avalanching plasmas and its meaning will be discussed elsewhere¹⁰. At least, as shown in figure 4(b) the T_e fluctuation near R_{av} has a long range temporal correlation (the Hurst exponent $H \sim 0.8$) in the time lag range of $0.1 < \tau < 1$ ms which corresponds to the frequency range of the power law spectrum $S(f) \propto f^{-0.7} \sim f^{1-2H}$. The Hurst exponent of the \tilde{T}_e is calculated using the rescaled range statistics (R/S)¹⁷ for $t = 3.8$ – 4.0 s. The large Hurst exponent ($H > 0.5$) over a broad radial region means superdiffusive characteristics of the electron heat transport in this plasma¹⁶.

As we mentioned earlier, the avalanche dynamics slightly changes in the $z_{\text{ECRH}} \sim z_{q=2}$ period. In the $z_{\text{ECRH}} > z_{q=2}$ period, the long range avalanche-like events occur when the T_e profile corrugations are destroyed and the broadband (0–75 kHz) C_{T_e} near R_{av} increases sharply with the local T_e increase. However, in the $z_{\text{ECRH}} \sim z_{q=2}$ period the \tilde{T}_e fluctuation spectrum is modified and onset of the avalanche-like event seems to be less relevant to the broadband \tilde{T}_e fluctuation power.

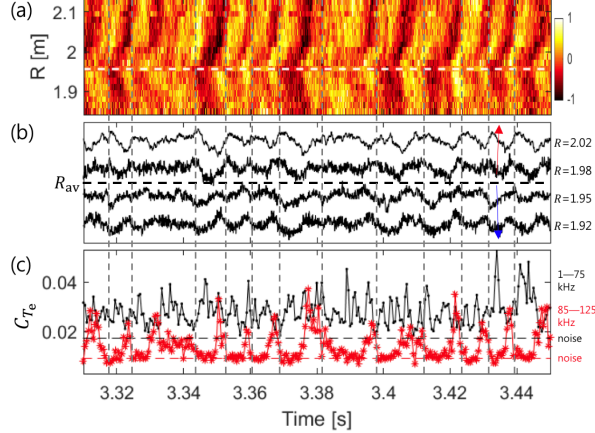


FIG. 6. (Color online) (a) The spatio-temporal pattern of the rescaled normalized T_e fluctuation in the $z_{\text{ECRH}} \sim z_{q=2}$ period. (b) The rescaled normalized T_e fluctuations at different R s. (c) Fast temporal evolution of the correlated T_e fluctuation powers in the 1–75 kHz (black dot) and 85–125 kHz (red asterisk) frequency band.

The spatio-temporal pattern of the rescaled \tilde{T}_e in the $z_{\text{ECRH}} \sim z_{q=2}$ period is shown in figure 6(a). 1D changes of T_e across R_{av} during the events are less ballistic and more complicated than in figure 2. 2D δT_e images during the avalanche-like event in the $z_{\text{ECRH}} \sim z_{q=2}$ period are similar with figure 3(c); the T_e profile corrugations and the $m = 1$ mode are observed after and before the event, respectively. However, the local T_e increase near R_{av} as in the frame #3 in figure 3(c) is rarely observed in this period, which may imply that trigger mechanism of the avalanche can be different.

In addition, the narrowband modes appear in the T_e fluctuation spectrum. The cross power spectrum in the $z_{\text{ECRH}} \sim z_{q=2}$ period ($t = 3.2$ – 3.5 s) is shown (red) in figure 7(a) together with that in the $z_{\text{ECRH}} > z_{q=2}$ period (black). Main mode of the narrowband modes is in the 105–125 kHz lobe and two side modes in the 84–102 kHz and 125–143 kHz lobes, respectively. Then, onset of the avalanche-like events is now synchronized with increase of the narrowband fluctuation power rather than the broadband fluctuation power. Figure 6(c) shows fast temporal evolution of C_{T_e} from the 1–75 kHz (black) and 85–125 kHz (red) \tilde{T}_e signals. Note that there is a small coherent electronics noise peak in the 130–135 kHz frequency band and so the 125–143 kHz side mode was excluded in the amplitude measurement. Significant increase of the 85–125 kHz C_{T_e} is observed before the events occur. Different characteristics of the onset-associated-fluctuation may result in different the

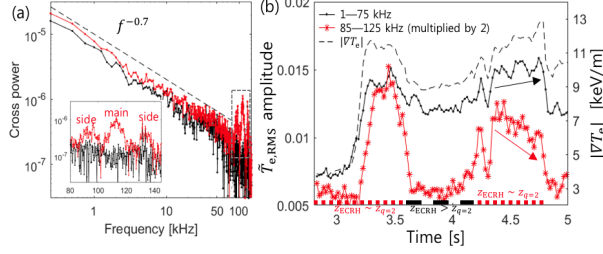


FIG. 7. (Color online) (a) The cross power spectrum measured by two adjacent ECEI channels in the $z_{\text{ECRH}} \sim z_{q=2}$ period (red) and the $z_{\text{ECRH}} > z_{q=2}$ period (black). (b) Time evolution of the broadband (black dot) and narrowband (red asterisk) $\tilde{T}_{e,\text{RMS}}$ with the local $|\nabla T_e|$ just inside R_{av} .

avalanche dynamics.

As a final remark about the observation, the broadband and narrowband fluctuations evolve in the opposite way with respect to the temperature gradient or the z_{ECRH} . In figure 7(b), slow temporal evolution of the $\tilde{T}_{e,\text{RMS}}$ and the electron temperature gradient ($|\nabla T_e|$) at $R = 1.96$ m ($R_{\text{av}} = 1.97$ m) are shown. The $\tilde{T}_{e,\text{RMS}}$ can be calculated averaging 50 ensembles of the cross power spectrum over 50 ms, and the noise contribution is significantly reduced. A significant narrowband $\tilde{T}_{e,\text{RMS}}$ above the noise level is detected when the broadband fluctuation amplitude and the $|\nabla T_e|$ are larger than some critical values with $z_{\text{ECRH}} \sim z_{q=2}$. However, once the narrowband fluctuation is excited, it evolves differently. For $t = 4.4\text{--}4.8$ s, the narrowband $\tilde{T}_{e,\text{RMS}}$ decreases in time as the broadband $\tilde{T}_{e,\text{RMS}}$ increases.

Beyond the avalanche dynamics, there remains important questions to be addressed more. First, finding physical origin of the T_e fluctuations will be important for further understandings of the dynamics such as formation mechanisms of the T_e profile corrugations and the $m = 1$ mode. While nonlinear gyrokinetic simulation for more understanding and cross validation of the experimental observations is in progress, the linear gyrokinetic simulation using GYRO has been performed in this plasma. It shows that the trapped electron mode (TEM) is strongly unstable in this plasma. Second, in the experiment the R_{av} position is found to be close to the $q = 2$ flux surface which also corresponds to the large $|\nabla T_e|$ position. Possible role of the rational surface in the avalanche dynamics will be studied in future q scan experiments.

In summary, the long range avalanche-like electron heat transport events are observed in the L-mode tokamak plasma when the significant MHD instabilities are absent. Detail

2D T_e measurements have revealed the complicated avalanche dynamics, which reasonably agrees with the gyrokinetic simulations. During the avalanching period, the common ∇T_e -correlated-fluctuation with the power law spectrum $S(f) \propto f^{-0.7}$ is identified with the Hurst exponent $H \sim 0.8$, which suggests that the electron heat transport is dominated by the nondiffusive avalanche-like events. Slight modification of the T_e fluctuation spectrum results in different trigger process of the avalanche-like event.

ACKNOWLEDGMENTS

M.J. Choi acknowledges helpful discussions with Dr. W. Wang, Prof. Y. Kishimoto, and Dr. K. Ida during the 4th UNIST-Kyoto workshop. This research was supported by the Ministry of Science and ICT of the Republic of Korea and the KSTAR Project Contract.

REFERENCES

- ¹P. H. Diamond and T. S. Hahm, “On the dynamics of turbulent transport near marginal stability,” *Physics of Plasmas* **2**, 3640–3649 (1995).
- ²X. Garbet and R. E. Waltz, “Heat flux driven ion turbulence,” *Physics of Plasmas* **5**, 2836–2845 (1998).
- ³Y. Idomura, H. Urano, N. Aiba, and S. Tokuda, “Study of ion turbulent transport and profile formations using global gyrokinetic full-f Vlasov simulation,” *Nuclear Fusion* **49**, 065029 (2009).
- ⁴B. F. McMillan, S. Jolliet, T. M. Tran, L. Villard, A. Bottino, and P. Angelino, “Avalanchelike bursts in global gyrokinetic simulations,” *Physics of Plasmas* **16**, 022310 (2009).
- ⁵Y. Sarazin, V. Grandgirard, J. Abiteboul, S. Allfrey, X. Garbet, P. Ghendrih, G. Latu, A. Strugarek, and G. Dif-Pradalier, “Large scale dynamics in flux driven gyrokinetic turbulence,” *Nuclear Fusion* **50**, 054004 (2010).
- ⁶G. Dif-Pradalier, P. H. Diamond, V. Grandgirard, Y. Sarazin, J. Abiteboul, X. Garbet, P. Ghendrih, A. Strugarek, S. Ku, and C. S. Chang, “On the validity of the local diffusive paradigm in turbulent plasma transport,” *Physical Review E* **82**, 025401(R) (2010).
- ⁷W. Wang, Y. Kishimoto, K. Imadera, J. Q. Li, and Z. X. Wang, “A mechanism for

- the formation and sustainment of the self-organized global profile and $E \times B$ staircase in tokamak plasmas,” *Nuclear Fusion* **58**, 056005 (2018).
- ⁸L. Qi, to be submitted.
- ⁹P. A. Politzer, “Observation of Avalanchelike Phenomena in a Magnetically Confined Plasma,” *Physical Review Letters* **84**, 1192–1195 (2000).
- ¹⁰M. J. Choi and J. Hogun, to be submitted.
- ¹¹J. G. Bak, S. G. Lee, and D. Son, “Performance of the magnetic sensor and the integrator for the kstar magnetic diagnostics,” *Review of Scientific Instruments* **75**, 4305–4307 (2004), <https://doi.org/10.1063/1.1789620>.
- ¹²Y. Kogi, S. H. Jeong, K. D. Lee, K. Akaki, A. Mase, D. Kuwahara, T. Yoshinaga, Y. Nagayama, M. Kwon, and K. Kawahata, “Calibration of electron cyclotron emission radiometer for kstar,” *Review of Scientific Instruments* **81**, 10D916 (2010), <https://doi.org/10.1063/1.3491304>.
- ¹³W. H. Ko, S. Oh, and M. Kwon, “Kstar charge exchange spectroscopy system,” *IEEE Transactions on Plasma Science* **38**, 996–1000 (2010).
- ¹⁴G. S. Yun, W. Lee, M. J. Choi, J. Lee, M. Kim, J. Leem, Y. Nam, G. H. Choe, H. K. Park, H. Park, D. S. Woo, K. W. Kim, C. W. Domier, N. C. Luhmann, N. Ito, A. Mase, and S. G. Lee, “Quasi 3-D ECE Imaging System for Study of MHD instabilities in KSTAR,” *Review of Scientific Instruments* **85**, 11D820 (2014).
- ¹⁵G. Dif-Pradalier, G. Hornung, X. Garbet, P. Ghendrih, V. Grandgirard, G. Latu, and Y. Sarazin, “The $E \times B$ staircase of magnetised plasmas,” *Nuclear Fusion* **57**, 066026 (2017).
- ¹⁶R. Sanchez and D. E. Newman, “Self-organized criticality and the dynamics of near-marginal turbulent transport in magnetically confined fusion plasmas,” *Plasma Physics and Controlled Fusion* **57**, 123002 (2015).
- ¹⁷B. A. Carreras, B. P. van Milligen, M. A. Pedrosa, R. Balbín, C. Hidalgo, D. E. Newman, E. Sánchez, M. Frances, I. García-Cortés, J. Bleuel, M. Endler, S. Davies, and G. F. Matthews, “Long-Range Time Correlations in Plasma Edge Turbulence,” *Physical Review Letters* **80**, 4438–4441 (1998).